INTERNATIONAL JOURNAL FOR NUMERICAL METHODS IN FLUIDS, VOL. 26, 79–100 (1998)

SECOND-ORDER MODEL FOR FREE SURFACE CONVECTION AND INTERFACE RECONSTRUCTION

SEONG-O. KIM[1]* AND HEE CHEON NO[2]

[1] *Advanced Reactor Development Department, Korea Atomic Energy Research Institute, (KAERI), PO Box 105, Yuseong, Taejeon 305–600, South Korea;*
[2] *Korea Advanced Institute of Science and Technology, South Korea*

SUMMARY

To improve the numerical analysis of free surface convection and interface reconstruction, both first- and second-order algorithms are developed based on the volume-of-fluid method. The methodology applied to the second-order model is to define the second-order linear curve having both face slopes as near horizontal as possible while satisfying the cell's defined volume fraction.

The second-order method is compared with the FLAIR method and the first-order method through simulation of the convection for various sizes of circular liquid shapes and solitary waves. For small curvature of the free surface, e.g. circles with large diameter, linear methods such as the FLAIR method and the first-order method show relatively good predictions. However, for large-curvature configurations, e.g. circles with relatively small diameter or solitary waves, the linear approach shows large distortion of the free surface. In contrast, the second-order model always shows powerful prediction capabilities of free surface convection. © 1998 John Wiley & Sons, Ltd.

Int. J. Numer. Meth. Fluids, **26**: 79–100 (1998)

KEY WORDS: volume-of-fluid method; free surface flows; second-order model

1. INTRODUCTION

1.1. General concept of free surface tracking

A variety of physical hydrodynamic phenomena involve interfaces between phases as shown in Figure 1(a) (where F and V denote a cell filled with fluid and a completely void cell respectively and S denotes a surface cell partially filled with fluid and partially void). These interfaces can exhibit dynamic behaviour and an exact mathematical description of the fluid interfaces is required to solve the transport equations of motion in the fluid domain. However, the numerical description of free surface flow and interfaces is notoriously complicated owing to difficulties associated with the discrete representation of the interfaces. The locations of these interfaces are not known in advance and must be determined as part of the solution of the transport equations.

There are several numerical methods for treating fluid problems with interfaces using the Lagrangian approach, such as boundary integral techniques,[1–3] finite element methods[4–6] and

Correspondence to: S.-O. Kim, Advanced Reactor Development Department, Korea Atomic Energy Research Institute, (KAERI), PO Box 105, Yuseong, Taejeon 305–600, South Korea. E-mail: sokin@nanum.kaeri.re.kr

CCC 0271–2091/98/010079–22 $17.50

Received 27 July 1995
Revised 1 March 1997

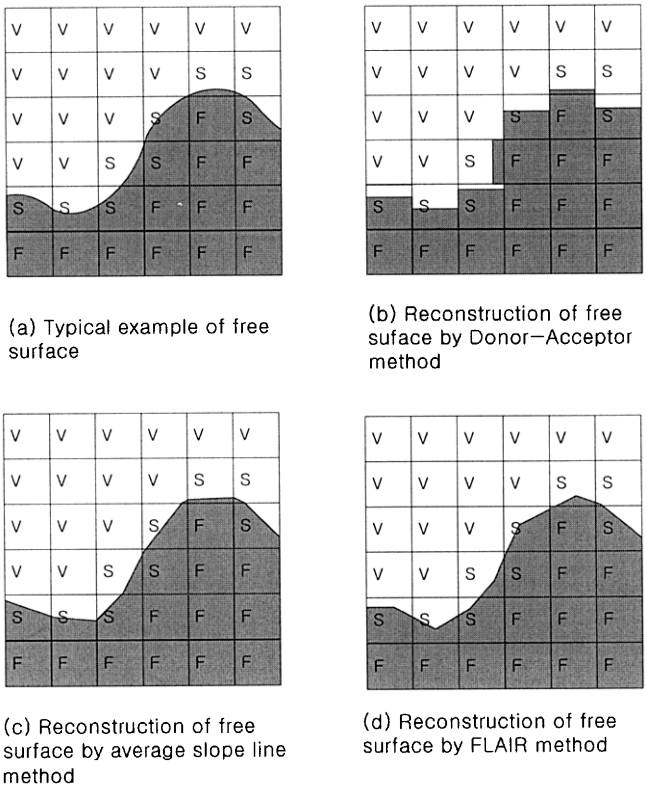

Figure 1. Typical example and reconstruction schemes for interfaces of free surface

boundary-fitted orthogonal co-ordinates.[7–9] Through these techniques the dynamic behaviour of free surfaces can be calculated prior to solving the momentum equation. However, it is difficult to handle complex phenomena such as surface folding and merging with these techniques owing to the requirement of discrete specification of the moving points.

A numerical technique that has the potential for handling large surface deformations as well as surface folding and merging is the volume-tracking method. This method uses a volumetric progress variable, such as marker particles in the marker-and-cell (MAC) technique[10–12] and the cell volume fraction technique,[13–16] for Lagrangian transport of the interfaces. The MAC method involves Eulerian flow field calculations and Lagrangian liquid–particle movements. The velocity of a marker is found by taking the average of the Eulerian velocities in its vicinity. One of the difficulties in using the MAC method is the possible creation of artificially high or low marker number densities in the cells owing to the irregularity of the flow field.

The volume-of-fluid (VOF) method can be applied to determine free surface curves by use of the volume fraction of a calculational cell and/or its neighbouring cells. This method is not susceptible to the problems which can be encountered when using the MAC method.

1.2. Review of VOF method

In earlier applications of the VOF method the donor–acceptor method of zeroth-order[17,18] was used for VOF advection calculation, where a surface cell was assumed to be of either horizontal or vertical

rectangular shape as shown in Figure 1(b). The decision on the orientation was made by studying the neighbouring cells. Once the surface orientation was identified, appropriate techniques could be used for its advection.[17,18] For instance, in the SLIC (simple line surface calculation) method of Noh and Woodward[16] the surface would be reconstructed for flux calculation as either a vertical or horizontal line in the x- or y-direction respectively. In the method of Hirt and Nichols[13] the surface orientation would also be considered to be either vertical or horizontal, but the calculation of the convective flux would be limited based on neighbouring volume fractions of the cell to prevent diffusion of the volume fraction owing to the excessive amount of advection.

However, the simple shape of the donor–acceptor technique introduces inaccuracies associated with the surface reconstruction and its advection in VOF convection. To improve the accuracy of free surface convection, two alternative approaches to the simple line method have been developed by Youngs[19] and Ashgriz and Poo,[20] where the interface is approximated by a sloped line in each cell rather than a horizontal or vertical line.

There is no detailed description of the procedure of Youngs' approach reported in the open literature for obtaining the slope of the surface cell and for calculating the convective flux of free surface flow. However, based on a review, the slope can be inferred to be defined as the average value of the slopes calculated at the cell centre as shown in Figure 1(c). In the FLAIR (flux line segment model for advection and interface reconstruction) method suggested by Ashgriz and Poo,[20] two kinds of convection methods are applied based on the status of the donor and acceptor cells. If both the adjacent cells are surface cells, the slope is calculated at the face located between the donor and acceptor cells. If one of the cells is a fluid cell or a void cell, the slope is calculated at the centre of the donor cell by use of the donor cell and its neighbouring cells as shown in Figure 1(d).

1.3. Necessity of a new model for free surface convection

In treating a free surface problem with wall boundary conditions, such as thin liquid layer flow, the major part of the velocity change usually occurs near the wall boundaries. To ensure accuracy of the momentum equation solution by a numerical method, a fine mesh distribution is generally required near the wall boundaries. However, a coarser mesh distribution may be allowed near the free surface, since the velocity distribution is nearly flat around the free surface.

When the interfaces of two different materials consist of complicated shapes, the mesh size around the interfaces must be fine enough to reconstruct the free surface correctly. This often leads to a fine mesh distribution over the whole computational domain. While this mesh distribution may bring good results for momentum and free surface convection calculation, an excessive calculation time may be required. In order to reduce the calculation time without impairing the calculational accuracy with a coarser mesh distribution, there is a need to develop a free convection model that can give improved predictions over conventional models.

Since there is no detailed information in the literature to describe Youngs' approach, the most accurate free surface convection model among the published ones seems to be the FLAIR method. The basic concept adopted in the FLAIR method is to assume that the interface can be represented as a straight line by segmenting the whole interface into small pieces. This approach could be appropriate when the system is segmented into small pieces. However, when the mesh distribution is not fine enough to be able to represent the interface with a straight line, the FLAIR method can construct inappropriate shapes for some cases as shown in Figure 2. Such shapes can often appear around the corners of the free surface even though the interface is segmented into small pieces. These inappropriate shapes can adversely affect the accuracy of the free surface convection model owing to the strong dependence of free surface convection on the slope at the convection face of the surface cell.

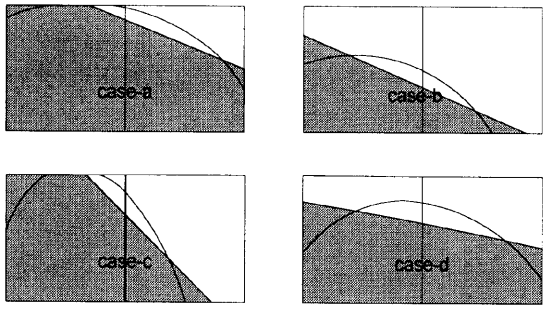

Figure 2. Typical examples of free surface reconstruction by FLAIR method

Although there is no general description of the accuracy of the free surface convection model, it is known that the accuracy of convection calculation for free surfaces depends not only on the slope of the convection face of the surface cell but also on the slope of the other face where the interfaces meet. To better represent the surface cells, a higher-order equation is needed to model the interfaces. This higher-order approximation can represent the interfaces more accurately but can require more computer time for convective flux calculation and a complicated solution procedure.

Despite the merits of high-order equations, if a higher-than-second-order approximation is used for modelling the free surface interfaces, the integration of the distribution function is higher than third-order, which is hard to solve analytically. The third-order integration equation generated from the second-order model can, however, be solved by analytical solution procedures.[21] Therefore a second-order approximation technique will be developed in this study.

2. SECOND-ORDER MODEL

The methodology applied for the second-order model is to find a second-order linear curve to fit the volume fraction distribution in a computational cell. The procedure for constructing the second-order model for the interfaces and calculating the convective flux is as follows.

Step 1. By inspecting the direction of a face velocity, define the cell block with the donor cell and its neighbouring cells as shown in Figure 3.
Step 2. Calculate the volume fraction slopes m_R, m_L, m_B and m_T at each cell face and determine the average slopes $(df/dX)_{AVG}$ and $(df/dY)_{AVG}$ and the slope change rates d^2f/dX^2 and d^2f/dY^2 in the X- and Y-direction respectively as described in Section 2.1.
Step 3. Rearrange the surface cell such that the nearly horizontal interfaces of the free surface lie along the x-direction of the model computational domain and reset the volume fraction such that the second-order curve has a convex shape in the positive y-direction of the model computational domain as described in Section 2.2.
Step 4. Define a normalized second-order linear equation and identify the base cases of the second-order model as described in Section 2.3.
Step 5. Identify the direction of convection and calculate the convective flux as described in Section 2.4.

2.1. Slope calculation

For calculating the slope at the face of a surface cell by use of neighbouring cells, it is assumed that the interface of the free surface can be represented by a single-valued function $f(X)$ or $f(Y)$ in the X-

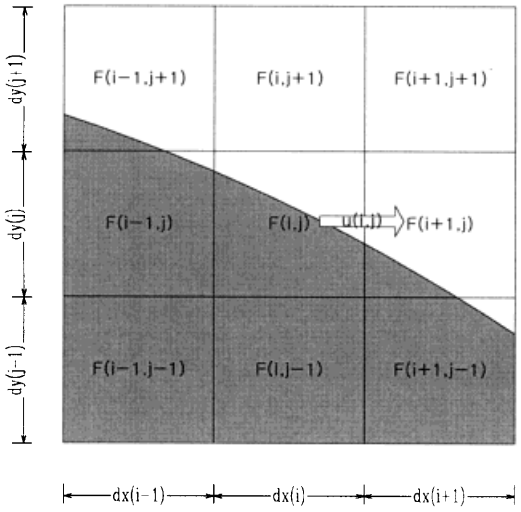

Figure 3. Definition of cell block

or Y-direction of the real computational domain. If the surface is represented as $f(X)$, $f(X)$ can be approximated as the sum of the volume fractions of cells $j-1$ to $j+1$ for each cell column of Figure 3:

$$f_{i-1} = \frac{\sum_{k=j-1}^{j+1} (\mathrm{d}y_k F_{i-1,k})}{H}, \tag{1}$$

$$f_i = \frac{\sum_{k=j-1}^{j+1} (\mathrm{d}y_k F_{i,k})}{H}, \tag{2}$$

$$f_{i+1} = \frac{\sum_{k=j-1}^{j+1} (\mathrm{d}y_k F_{i+1,k})}{H}, \tag{3}$$

where $H = \sum_{k=j-1}^{i+1} \mathrm{d}y_k$ and $f = 0$ are taken as the bottom edge of the $(j-1)$ row of cells. The slope of each face is determined by drawing a straight line ($f = mx + n$) below which both liquid and void volume fractions are located. If the larger volume fraction between the two columns is assigned as F_{M} and the smaller one as F_{m} and if the cell width is represented as $x_{\mathrm{L}}(= L/H)$ for F_{M} and $x_{\mathrm{R}}(= R/H)$ for F_{m} as shown in Figure 4, then the boundary slope m is calculated from equation (4)–(7) by categorizing the cases based on the values of $f_{\mathrm{M}}, f_{\mathrm{m}}, x_{\mathrm{L}}$ and x_{R} as shown in Figure 2:

Case 1

$$m = \frac{2}{x_{\mathrm{L}}^2}\{-(2x_{\mathrm{R}}F_{\mathrm{m}} + x_{\mathrm{L}}F_{\mathrm{M}}) + 2\sqrt{[x_{\mathrm{R}}F_{\mathrm{m}}(x_{\mathrm{R}}F_{\mathrm{m}} + x_{\mathrm{L}}F_{\mathrm{M}})]}\} \tag{4}$$

$$\text{if} \quad F_{\mathrm{m}} \geqslant \frac{x_{\mathrm{R}}F_{\mathrm{M}}}{2x_{\mathrm{R}} + x_{\mathrm{L}}} \quad \text{and} \quad x_{\mathrm{L}}(1 - F_{\mathrm{M}}) + \sqrt{[F_{\mathrm{m}}(1 - F_{\mathrm{M}})x_{\mathrm{L}}x_{\mathrm{R}}]} \geqslant \frac{x_{\mathrm{L}}}{2};$$

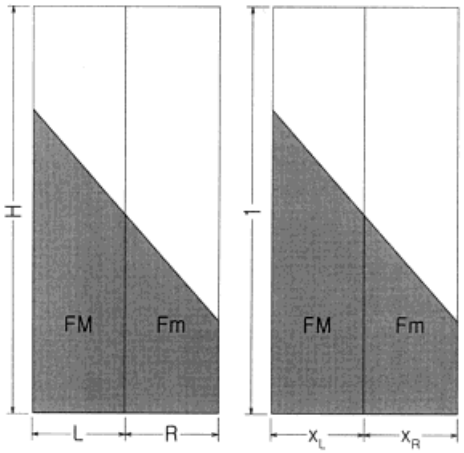

Figure 4. Calculation of volume fraction slope between two cell columns

Case 2

$$m = \frac{2(F_m - F_M)}{x_R + x_L} \tag{5}$$

$$\text{if} \quad F_m \geqslant \frac{x_R F_M}{2x_R + x_L} \quad \text{and} \quad F_m \geqslant \frac{F_M(x_R + 2x_L) - (x_R + x_L)}{x_L};$$

Case 3

$$m = -\frac{1}{2\{F_m x_R + \sqrt{[F_m(1 - F_M)x_R x_L]}\} + 2\{(1 - F_M)x_L + \sqrt{[F_m(1 - F_M)x_R x_L]}\}} \tag{6}$$

$$\text{if} \quad x_L(1 - F_M) + \sqrt{[F_m(1 - F_M)x_L x_R]} \leqslant \frac{x_L}{2} \quad \text{and} \quad x_R f_m + \sqrt{[F_m(1 - F_M)x_R x_L]} \leqslant \frac{x^R}{2};$$

Case 4

$$m = \frac{-2}{x_R^2}[[2x_L(1 - F_M) + x_R(1 - F_m) + 2\sqrt{\{x_L(1 - F_M)[x_L(1 - F_M) + x_R(1 - F_m)]\}}]] \tag{7}$$

$$\text{if} \quad F_m \leqslant \frac{F_M(x_R + 2x_L) - (x_R + x_L)}{x_L} \quad \text{and} \quad x_R F_m + \sqrt{[F_m(1 - F_M)x_R x_L]} \geqslant \frac{x_R}{2}.$$

From the slopes of boundary faces the average slope and the slope change rate are calculated by

$$\left(\frac{df}{dX}\right)_{AVG} = \frac{m_R \delta x_L + m_l \delta x_R}{\delta x_R + \delta x_L}, \tag{8}$$

$$\frac{d^2 f}{dX^2} = \frac{m_R - m_L}{\delta x_R + \delta x_L}, \tag{9}$$

where

$$\delta x_{\mathrm{R}} = \frac{\mathrm{d}x_i + \mathrm{d}x_{i+1}}{2H}, \qquad \delta x_{\mathrm{L}} = \frac{\mathrm{d}x_{i-1} + \mathrm{d}x_i}{2H}.$$

A similar calculation can be made for $\mathrm{d}f/\mathrm{d}Y$, i.e.

$$f_{j-1} = \sum_{k=i-1}^{i+1} (\mathrm{d}x_k F_{k,j-1}), \tag{10}$$

$$f_j = \sum_{k=i-1}^{i+1} (\mathrm{d}x_k F_{k,j}), \tag{11}$$

$$f_{j+1} = \sum_{k=i-1}^{i+1} (\mathrm{d}x_k F_{k,j+1}), \tag{12}$$

$$\left(\frac{\mathrm{d}f}{\mathrm{d}Y}\right)_{\mathrm{AVG}} = \frac{m_{\mathrm{T}}\delta y_{\mathrm{B}} + m_{\mathrm{B}}\delta y_{\mathrm{T}}}{\delta y_{\mathrm{T}} + \delta y_{\mathrm{B}}}, \tag{13}$$

$$\frac{\mathrm{d}^2 f}{\mathrm{d}Y^2} = \frac{m_{\mathrm{T}} - m_{\mathrm{B}}}{\delta y_{\mathrm{T}} + \delta y_{\mathrm{B}}}, \tag{14}$$

$$\delta y_{\mathrm{T}} = \frac{\mathrm{d}y_j + \mathrm{d}y_{j+1}}{2H}, \qquad \delta y_{\mathrm{B}} = \frac{dy_{j-1} + dy_j}{2H}, \tag{15}$$

where $H = \sum_{k=i-1}^{i+1} \mathrm{d}x_k$ and $f = 0$ are taken as the bottom edge of the $(j-1)$th row of cells (Figure 2a).

2.2. *Rearrangement of surface cell block*

When an arbitrary surface cell block is defined from a typical interface as shown in Figure 3, there are a variety of free surface shapes around the donor cell as shown in Figure 5. To reduce the number of cases, neighbouring cells must be rearranged. First, the cell block is rotated such that the nearly horizontal orientation of the interface lies along the x-direction of the model computational domain, where the horizontal orientation is defined as the direction with the smaller absolute magnitude of average slope. By this manipulation, Cases 5–8 and 13–16 in Figure 5 can be eliminated. If the liquid phase lies above the convex line of the second-order curve, the volume fraction is redefined for void instead of liquid. With this redefinition of volume fraction, Cases 9–12 are identical to Cases 1–4 in Figure 5. Finally, by examining the average slope of Cases 1–4 in the x- and y-direction, the volume fractions of the left and right columns or those of the top and bottom rows are interchanged so that the sum of volume fractions of the left column and that of the bottom row have a larger value than the others. Using this procedure of neighbouring cell rearrangement and volume fraction resetting all the cases in Figure 5 can be represented by a single case, i.e. Case 1. Also, all the slopes and volume fractions calculated in Section 2.1 are rearranged to have the shape of Case 1 in Figure 5. The detailed data are given in Table I.

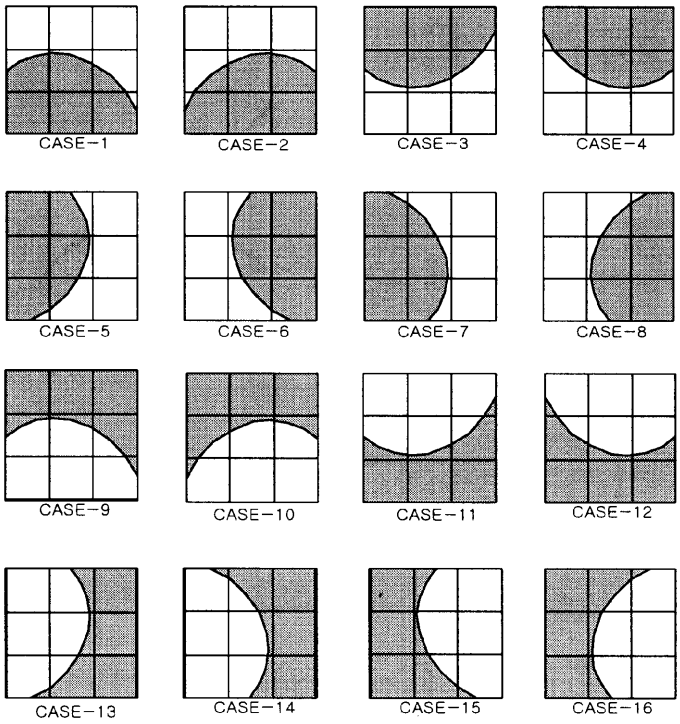

Figure 5. Possible volume fraction distributions in cell block

2.3. *Model case identification*

After rearrangement of the boundary cell block as described in Section 2.2, a second-order linear equation is defined to represent the volume fraction distribution in a surface cell normalized by the surface cell height H and width W:

$$y = ax^2 + bx + c. \tag{16}$$

The constants a and b are obtained by differentiating equation (16) and calculating the slopes of the left and right faces of a surface cell via the equations

$$a = \frac{m_r - m_l}{2}, \qquad b = m_l, \tag{17}$$

$$m_r = \frac{W}{H} m'_R, \qquad m_l = \frac{W}{H} m'_L \tag{18}$$

where m'_R and m'_L are the slopes defined in Table I.

When fitting the interfaces of a surface cell by the second-order curve, eight possible shapes may exist as shown in Figure 6. However, Cases f–h can be eliminated by restricting the maximum difference in volume fraction distribution within a cell to less than the cell height, because Cases f–h rarely appear in volume fraction calculations of the rearranged interface. Furthermore, higher-than-fourth-order algebraic equations have to be solved to get the constant c of equation (16) for Cases f–h.

The maximum cell difference within a surface cell can be defined by two types. If the slopes m_r and m_l have the same sign, the maximum difference is the distance between the intersecting points f_l

Table I. Information on second-order model: slopes, VOF definitions and convection directions (x and y, co-ordinates of model; X and Y, co-ordinates of calculational domain; $m_x = (\mathrm{d}f/\mathrm{d}X)_{\mathrm{AVG}}$; $m_Y = (\mathrm{d}f/\mathrm{d}Y)_{\mathrm{AVG}}$; $a = (\mathrm{d}^2f/\mathrm{d}X^2)$ if $|m_X| > |m_Y|$; $a = (\mathrm{d}^2f/\mathrm{d}Y^2)$ if $|m_X| < |m_Y|$)

$\lvert m_X\rvert - \lvert m_Y\rvert$	a	m_Y	m_X	m'_{L}	m'_{R}	x	y	Definition of VOF	Case number of Figure 5
<0	<0	<0	<0	$+m_{\mathrm{L}}$	$+m_{\mathrm{R}}$	X	Y	Fluid	1
<0	<0	<0	>0	$-m_{\mathrm{R}}$	$-m_{\mathrm{L}}$	$-X$	Y	Fluid	2
<0	<0	>0	<0	$+m_{\mathrm{L}}$	$+m_{\mathrm{R}}$	X	$-Y$	Fluid	3
<0	<0	>0	>0	$-m_{\mathrm{R}}$	$-m_{\mathrm{L}}$	$-X$	$-Y$	Fluid	4
>0	<0	>0	<0	$-m_{\mathrm{T}}$	$-m_{\mathrm{B}}$	$-Y$	X	Fluid	5
>0	<0	>0	>0	$-m_{\mathrm{T}}$	$-m_{\mathrm{B}}$	$-Y$	$-X$	Fluid	6
>0	<0	<0	<0	$+m_{\mathrm{B}}$	$+m_{\mathrm{T}}$	Y	X	Fluid	7
>0	<0	<0	>0	$+m_{\mathrm{B}}$	$+m_{\mathrm{T}}$	Y	$-X$	Fluid	8
<0	>0	>0	>0	$-m_{\mathrm{L}}$	$-m_{\mathrm{R}}$	X	Y	Void	9
<0	>0	>0	<0	$+m_{\mathrm{R}}$	$-m_{\mathrm{L}}$	$-X$	Y	Void	10
<0	>0	<0	>0	$-m_{\mathrm{L}}$	$-m_{\mathrm{R}}$	X	$-Y$	Void	11
<0	>0	<0	<0	$+m_{\mathrm{R}}$	$-m_{\mathrm{L}}$	$-X$	$-Y$	Void	12
>0	>0	<0	>0	$+m_{\mathrm{T}}$	$+m_{\mathrm{B}}$	$-Y$	X	Void	13
>0	>0	<0	<0	$+m_{\mathrm{T}}$	$+m_{\mathrm{B}}$	$-Y$	$-X$	Void	14
>0	>0	>0	>0	$-m_{\mathrm{B}}$	$-m_{\mathrm{T}}$	Y	X	Void	15
>0	>0	>0	<0	$-m_{\mathrm{B}}$	$-m_{\mathrm{T}}$	Y	$-X$	Void	16

and f_{r} of the left and right faces of the cell as defined in Figure 7. However, if the slopes m_{r} and m_{l} have different signs, the maximum difference is the distance from the polar value f_{p} to the intersection point f_{r} of the right face. If the maximum difference exceeds the cell height, the cell slope is corrected so that the difference will be the same as the cell height as follows:

$$m_{\mathrm{r}} = -\frac{2H}{W}\frac{m'_{\mathrm{R}}}{m'_{\mathrm{R}} + m'_{\mathrm{L}}} \quad \text{and} \quad m_{\mathrm{l}} = \frac{m'_{\mathrm{L}}}{m'_{\mathrm{R}}} m_{\mathrm{r}} \quad \text{if} \quad m'_{\mathrm{L}} m'_{\mathrm{R}} \geqslant 0, \tag{19}$$

$$m_{\mathrm{r}} = -\frac{2H}{W}\frac{m'_{\mathrm{L}} - m'_{\mathrm{R}}}{m'_{\mathrm{R}}} \quad \text{and} \quad m_{\mathrm{l}} = \frac{m'_{\mathrm{L}}}{m'_{\mathrm{R}}} m_{\mathrm{r}} \quad \text{if} \quad m'_{\mathrm{L}} m'_{\mathrm{R}} \leqslant 0. \tag{20}$$

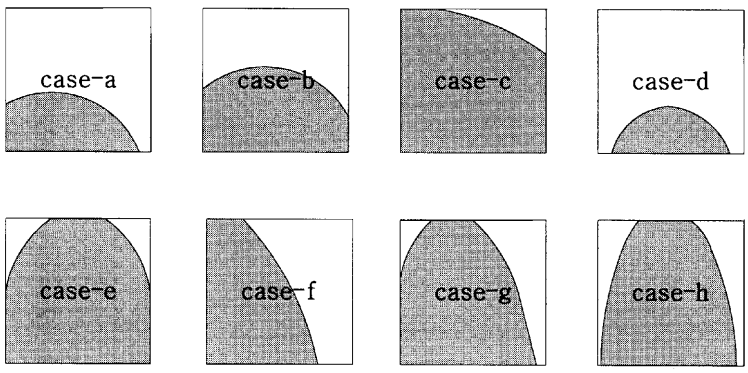

Figure 6. Possible interface shapes in approximating free surface by second-order model

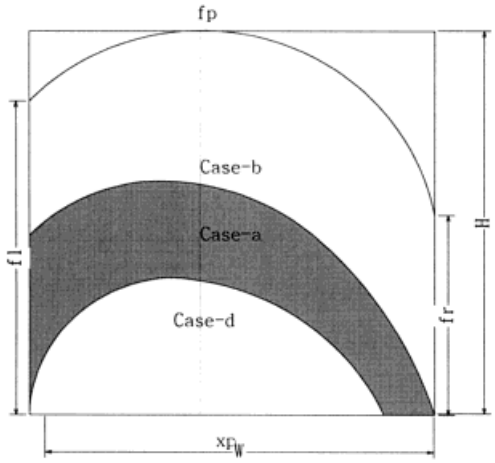

Figure 7. Boundaries for Cases a, b and d of second-order model

After adjusting the boundary slope, the second-order model is categorized into five cases (Cases a–e). To calculate the constant of equation (16) and the convective flux, every case must be examined. Each case is examined by comparing the real volume fraction F with the area which is calculated by setting one of the intersection points f_l and f_r of the left and right faces or the peak value f_p located within the surface cell range to zero or the cell height of Figure 7. For instance, to differentiate Case a from Cases b and d, two criteria must be established. The criterion to differentiate Case a from Case b is first established by setting the intersection points f_r of the right face to zero and integrating equation (16) from $x = 0$ to 1:

Case a

$$\text{if} \quad F \leqslant -\frac{2m_r + m_l}{6}; \tag{21}$$

Case b

$$\text{if} \quad F \geqslant -\frac{2m_r + m_l}{6}. \tag{22}$$

The second criterion is established to differentiate Case a from Case d. As the slope of the left face is less than that of the right face, the polar point x_p is located nearer the left face. Therefore the criterion is established as follows by setting the intersection point f_l of the left face to zero as shown in Figure 7:

Case a

$$\text{if} \quad F \geqslant \frac{m_l^3}{6(m_r - m_l)^3}; \tag{23}$$

Case b

$$\text{if} \quad F \leqslant \frac{m_l^3}{6(m_r - m_l)^3}. \tag{24}$$

By similar evaluations, all the cases can be examined via the following criteria:

Case a

$$\text{if} \quad F \geqslant \frac{m_l^3}{(m_l - m_r)^3} \quad \text{and} \quad F \leqslant -\frac{2m_r + m_l}{6}; \tag{25}$$

Case b

$$\text{if} \quad F \geqslant -\frac{2m_r + m_l}{6} \quad \text{and} \quad F \leqslant 1 - \frac{m_l^3 - m_r^3}{(m_l - m_r)^2}; \tag{26}$$

Case c

$$\text{if} \quad F \geqslant 1 + \frac{m_r + 2m_l}{6} \quad \text{for} \quad m_l m_r \geqslant 0, \tag{27}$$

$$\text{if} \quad F \geqslant 1 + \frac{m_r - 2m_l}{6}\left(\frac{m_r - m_l}{m_r + m_l}\right)^2 \quad \text{for} \quad m_r m_l \leqslant 0; \tag{28}$$

Case d

$$\text{if} \quad F \leqslant \frac{m_l^3}{6(m_r - m_l)^3}; \tag{29}$$

Case e

$$\text{if} \quad F \geqslant 1 - \frac{m_l^3 - m_r^3}{(m_l - m_r)^2} \quad \text{and} \quad F \leqslant 1 + \frac{m_r - 2m_l}{6}\left(\frac{m_r - m_l}{m_r + m_l}\right)^2. \tag{30}$$

2.4. Calculation of convective flux

For calculating the convective flux, the direction of convection in the calculational model must be identified, since the cell block is rearranged to reduce the number of cases. The details of the coordinates of x and y of the rearranged model relative to the directions X and Y of the real computational domain are given in Table I.

To calculate the convective flux, the constant c of equation (16) must be determined. For Cases b and d the constant c is determined explicitly as follows:

Case b

$$c = F - \frac{2m_r + m_l}{6}; \tag{31}$$

Case d

$$c = \frac{b^2}{4a} - \frac{a}{4}\left(-\frac{6F}{a}\right)^{2/3}. \tag{32}$$

However, for Cases a, c and e the constant c must be evaluated from the third-order algebraic equation which comes from integrating the second-order linear equation within the surface cell. As an example, the constant c of Case a will be calculated by equating the volume fraction value to that

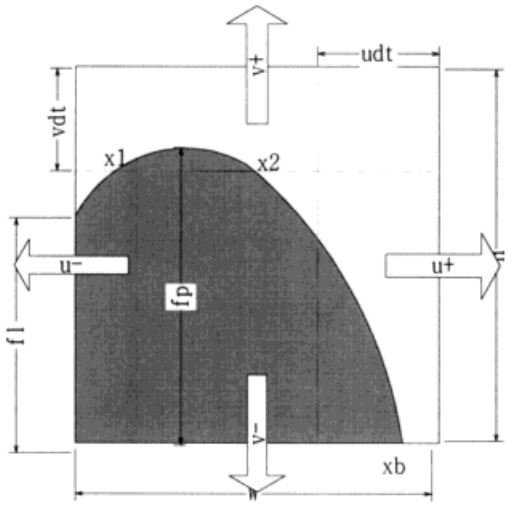

Figure 8. Calculation of second-order convective flux in each direction

integrated from the left face of the cell to the bottom point x_b of Figure 8. Proper manipulation yields the third-order algebraic equation

$$x_b^3 + \frac{3b}{4a}x_b^2 + \frac{3F}{2a} = 0. \tag{33}$$

After establishing the third-order algebraic equation, an appropriate solution is obtained by Cardano's solution procedure.[21] Letting $Q = -(b/4a)^2$, $R = -3F/4a - (b/4a)^3$ and $D = Q^3 + D^2$,

$$\text{if} \quad D \geqslant 0, \quad \text{then} \quad x_b = \sqrt{(R + \sqrt{D})} + \sqrt{(R - \sqrt{D})}. \tag{34}$$

$$\text{if} \quad D < 0, \quad \text{then} \quad x_1 = \frac{b}{a}\cos\left(\frac{\theta}{3}\right), \quad x_2 = \frac{b}{a}\cos\left(\frac{\theta}{3} + \frac{2\pi}{3}\right), \quad x_3 = \frac{b}{a}\cos\left(\frac{\theta}{3} + \frac{4\pi}{3}\right), \tag{35}$$

where $\theta = \cos^{-1}(D^2/Q^3)$ and x_b is the solution which exists within 0–1 from x_1, x_2 and x_3.

For Cases c and e the constant c can be obtained by a similar procedure to that for Case a.

The convective flux calculation in the second-order model is accomplished via integration of the second-order equation from the cell face to the distance defined by the local velocity of the cell face over time. For example, for Case a the fluid flux in the positive x-direction is

$$\delta f_{x+} = 0 \quad \text{if} \quad x_p \geqslant x_b, \tag{36}$$

$$\delta f_{x+} = \int_{x_p}^{x_b} f \, dx \quad \text{if} \quad x_p \leqslant x_b, \tag{37}$$

where $x_p = 1 - (u_+ \, dt)/W$. The fluid flux in the negative x-direction is

$$\delta f_{x-} = \int_0^{x_m} f \, dx \quad \text{if} \quad x_m \leqslant x_b, \tag{38}$$

$$\delta f_{x-} = F \quad \text{if} \quad x_m \geqslant x_b, \tag{39}$$

where $x_m = (u_- \, dt)/W$. The fluid flux in the positive y-direction is

$$\delta f_{y+} = 0 \quad \text{if} \quad y_p \geqslant f_p, \tag{40}$$

$$\delta f_{y+} = \int_{x_1}^{x_2} (f - y_p) \, dx \quad \text{if} \quad f_l \leqslant y_p \leqslant f_p, \tag{41}$$

$$\delta f_{y+} = \int_{0}^{x_2} (f - y_p) \, dx \quad \text{if} \quad y_p \leqslant f_p, \tag{42}$$

where $y_p = 1(v_+ \, dt)/H$ and x_1 and x_2 are the points where the second-order curve intersects the line $f = y_p$. The fluid flux in the negative y-direction is

$$\delta f_{y-} = F \quad \text{if} \quad y_m \geqslant f_p, \tag{43}$$

$$\delta f_{y-} = \int_{x_1}^{x_2} (f - y_m) \, dx \quad \text{if} \quad f_l \leqslant y_m \leqslant f_p, \tag{44}$$

$$\delta f_{y-} = \int_{0}^{x_2} (f - y_m) \, dx \quad \text{if} \quad y_m \leqslant f_l, \tag{45}$$

where $y_m = (v_- \, dt)/H$ and x_1 and x_2 are the points where the second-order curve intersects the line $f = y_m$.

3. FIRST-ORDER MODEL

As discussed in Section 1, there are two methods in the literature for calculating the convection of a free surface by use of the sloped line approach. The FLAIR method uses the face slope of the surface cell. Alternatively, the first-order approach (using the average slope of the surface cell) was introduced by Youngs, but the detailed methodology is not described. Thus a procedure is developed herein for the first-order method which is based on the average slope at the centre of the surface cell.

The basic concept of the first-order method is very similar to that of the second-order method in that the average slope of the horizontal orientation of a free surface is utilized for constructing the first-order linear curve. After rearranging the surface cell and neighbouring cells in the cell block and calculating the average slope in the same way as in the second-order method, four cases of the surface cell model are established as shown in Figure 9. To model the volume fraction in the surface cell by the first-order linear curve (equation (46)), the constant n is determined by setting the volume fraction value equal to the integrated value of the first-order curve for each case:

$$f = mx + n, \tag{46}$$

where m is the average slope of the cell face;

Case a

$$\text{if} \quad F \leqslant \frac{-m}{2} \quad \text{and} \quad F \leqslant \frac{1}{2m}, \quad \text{then} \quad n = \sqrt{(-2mF)}; \tag{47}$$

Case b

$$\text{if} \quad F \leqslant \frac{m}{2} + 1 \quad \text{and} \quad F \geqslant -\frac{m}{2}, \quad \text{then} \quad n = F - \frac{m}{2}; \tag{48}$$

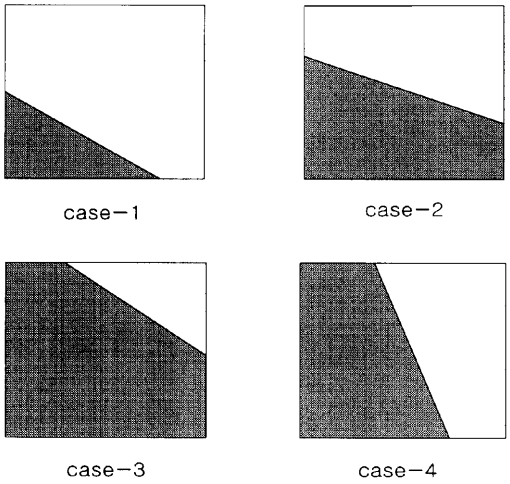

Figure 9. Possible cases of first-order method

Case c

$$\text{if} \quad F \geqslant \frac{m}{2} + 1 \quad \text{and} \quad F \geqslant 1 + \frac{1}{2m}, \quad \text{then} \quad n = 1 - m - \sqrt{[-2m(1-F)]}; \tag{49}$$

Case d

$$\text{if} \quad F \leqslant 1 + \frac{1}{2m} \quad \text{and} \quad F \geqslant -\frac{1}{2m}, \quad \text{then} \quad n = \tfrac{1}{2} - mF. \tag{50}$$

After the constants m and n have been fixed, the convective flux for each case can be determined by integration of the first-order linear curve from the surface cell face to the distance determined from the local velocity for each direction over time (Figure 10). As an example, the fluid flux in the positive x-direction for Case c is

$$\delta f_{x+} = \int_{x_p}^{1} f \, \mathrm{d}x \quad \text{if} \quad x_p \geqslant x_t, \tag{51}$$

$$\delta f_{x+} = x_t - x_p + \int_{x_t}^{1} f \, \mathrm{d}x \quad \text{if} \quad x_p \leqslant x_t, \tag{52}$$

where $x_p = 1 - (u_+ \mathrm{d}t)/W$. The fluid flux in the negative x-direction is

$$\delta f_{x-} = x_m \quad \text{if} \quad x_m \leqslant x_t, \tag{53}$$

$$\delta f_{x-} = x_m - x_t + \int_{0}^{x_t} f \, \mathrm{d}x \quad \text{if} \quad x_m \geqslant x_t, \tag{54}$$

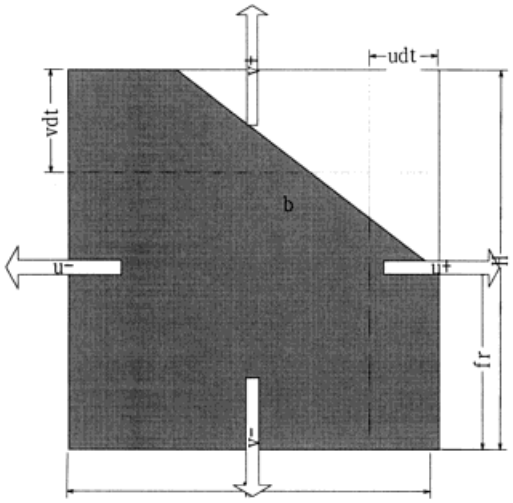

Figure 10. Schematic drawing of convective flux calculation of first-order method

where $x_m = (u_- \, dt)/W$. The fluid flux in the positive y-direction is

$$\delta f_{y+} = \int_{x_s}^{1} (f - y_p) \, dx \quad \text{if} \quad y_p \geqslant f_r, \tag{55}$$

$$\delta f_{y+} = \int_{0}^{x_s} (f - y_p) \, dx \quad \text{if} \quad y_p \leqslant f_r, \tag{56}$$

where $y_p = 1 - (v_+ \, dt)/H$ and x_s is the point where the first-order curve intersects the line y_p. The fluid flux in the negative y-direction is

$$\delta f_{y-} = y_m \quad \text{if} \quad y_m \geqslant f_r, \tag{57}$$

$$\delta f_{y-} = x_s y_m + \int_{x_s}^{1} f \, dx \quad \text{if} \quad y_m \leqslant f_r, \tag{58}$$

where $y_m = (v_- \, dt)/H$ and x_s is the point where the first-order curve intersects the line y_m.

4. RESULTS AND DISCUSSION

4.1. Case-by-case model comparison

To assess the capability for reconstruction of free surface shapes, four cases are compared as shown in Figure 11. The slopes of the left and right faces in Cases 1 and 2 have the same sign and the slopes of the left and right faces in Cases 3 and 4 have different signs. Comparing the capability for reconstruction of the free surface shape between the first-order method and the FLAIR method, the first-order method more accurately represents the analytic second-order curve for left and right convection than the FLAIR method for Cases 1 and 3. For Cases 2 and 4 the FLAIR method provides a better representation of the second-order curve in the right-hand direction but the first-order method fits the second-order curve in the left-hand direction. It is concluded that if the average slopes of the two adjacent cells have the same sign and the magnitudes are almost the same, the FLAIR method

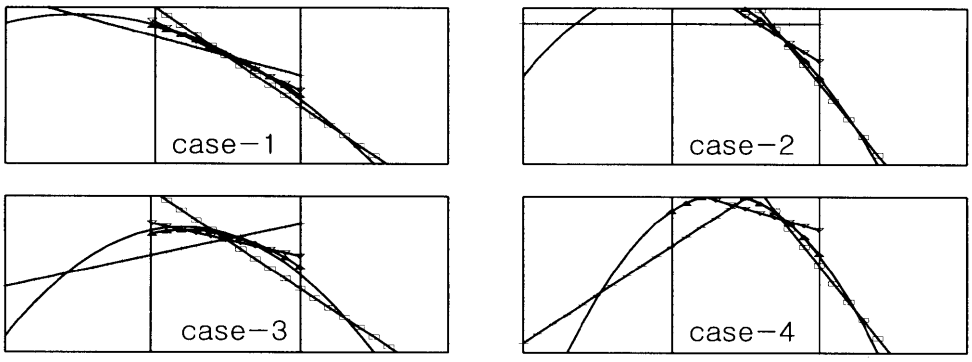

Figure 11. Shapes of reconstruced interface of free surface with large curvature by use of various free surface convection models. —, analytic input data; ⊟, FLAIR method for convection in right-hand direction; +, FLAIR method for convection in left-hand direction; ▽, first-order method; ▲, second-order method

more closely reconstructs the original shape. However, if the average slopes of the two adjacent cells have different signs and the difference in magnitudes is large, the FLAIR method yields poor results. Additionally, if the slope change rate is relatively small, the centre-averaged first-order method closely reconstructs the original shape. However, if the slope change rate is relatively large, the first-order approach also yields poor results. Therefore, to reproduce accurate representations of the original shape by the sloped line method, either of the methods should be applied only after verifying the slope change rate and the average slopes of two adjacent cells.

For cases 1–4 as shown in Figure 11, the second-order approach used in this study accurately reproduces the second-order analytic curve in all cases. The second-order approach shows accurate curve-fitting capability for the case of multiple connected boundary cells with large curvature.

4.2. Convection capability of a circle

Both models developed in this study are tested and compared with the FLAIR method for the convection of a circular geometry. Here the FLAIR method is implemented in two different approaches. First, it is done without special correction for the diffusion of volume fraction in the procedure of free surface convection in exactly the same way as in the first- and second-order methods. Second, the convection calculations of the free surface are done by the programme supplied by the original authors of the FLAIR method.[20] There are large amounts of correction logic to prevent the diffusion of volume fraction in that programme. A uniform velocity field is assigned for the entire calculational region in the right and upward direction. The velocities in the x- and y-direction are assigned as one-quarter of the minimum mesh size, which is unit length in this study. Each circular region is convected in this velocity for 100 time steps until the circle has moved completely out of its original position. The calculational results are reviewed for three types of numerical error. The first is the maximum cell convection error which can be an indication of local shape deformation. The second is the root of the square sum of every cell error for an indication of overall shape deformation. The final error is the total volume change to measure the conservation of volume fraction. The cell convection error is defined as the cell volume fraction difference divided by the total circle area, where the cell volume fraction difference means the value of the original analytic input data minus the value of the cell volume fraction after 100 time steps of convection for each cell.

The maximum cell errors for each convection method are shown in Figure 12. The first- and second-order approaches show a continuous decrease. However, both FLAIR method applications

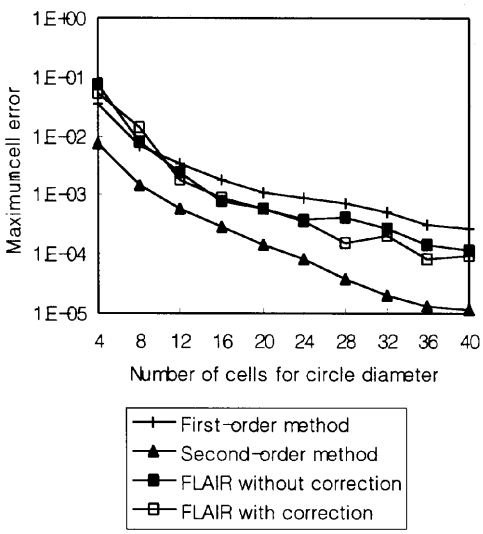

Figure 12. Maximum cell error versus circle diameter after 100 time steps of convection

show slight oscillations with the number of cells in the diameter of the circular geometry. The oscillation comes from the convection method of the FLAIR method. The flair method uses one of two convection methods according to the volume fraction status of donor and acceptor cells. If one of the volume fractions of two cells is full or void, the centre-averaged sloped line method (which is almost identical to the first-order approach described in this study except for the techniques of slope calculation) is used. If both volume fractions are not full or empty, the boundary sloped line techniques are used.

For the error magnitude the second-order method shows less error than the other methods at the same cell number of circle diameter. The results obtained from the FLAIR method both with and

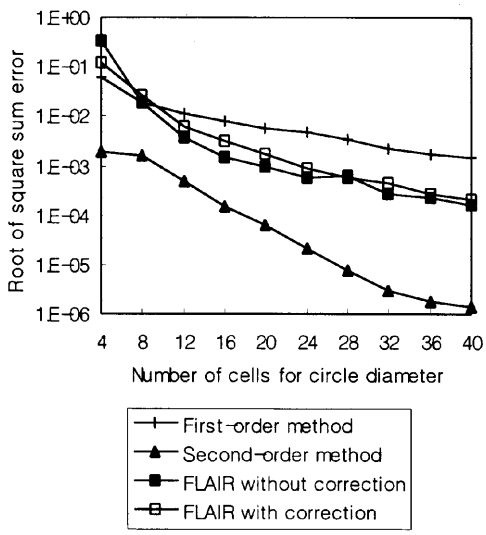

Figure 13. Root of square sum error versus circle diameter after 100 time steps of convection

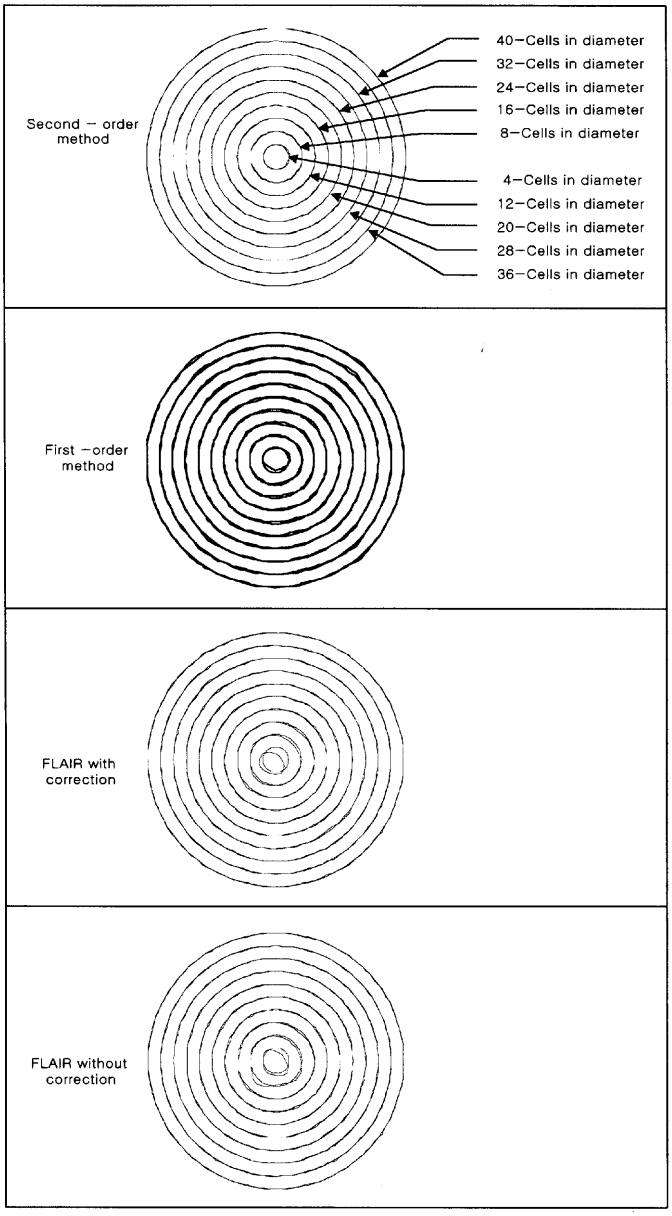

Figure 14. Reconstruction of circles after 100 time steps of convection by each free convection model

without correction logic show almost the same degree of accuracy and are better than the results of the first-order method.

When comparing the error slopes in the semilogarithmic plots of errors, it is known that the second-order method solutions converge more rapidly than those of the methods such as the first-order and the FLAIR method. It may be reasoned that a circle can be represented exactly by the segments of a second-order curve as the circle diameter increases, but a circle cannot be represented

exactly by the segments of a linear curve even if the diameter of the circle increases compared with the cell size.

The root of the square sum error for each technique has a similar tendency to the maximum cell error. Almost the same error magnitudes result as shown in Figures 12 and 13. This means that most cell convection errors are very small except for the cells that have the dominant error.

Considering both the maximum cell error and root of square sum error results the second-order model shows an equivalent error magnitude as compared with the first-order approaches with almost half the number of cells.

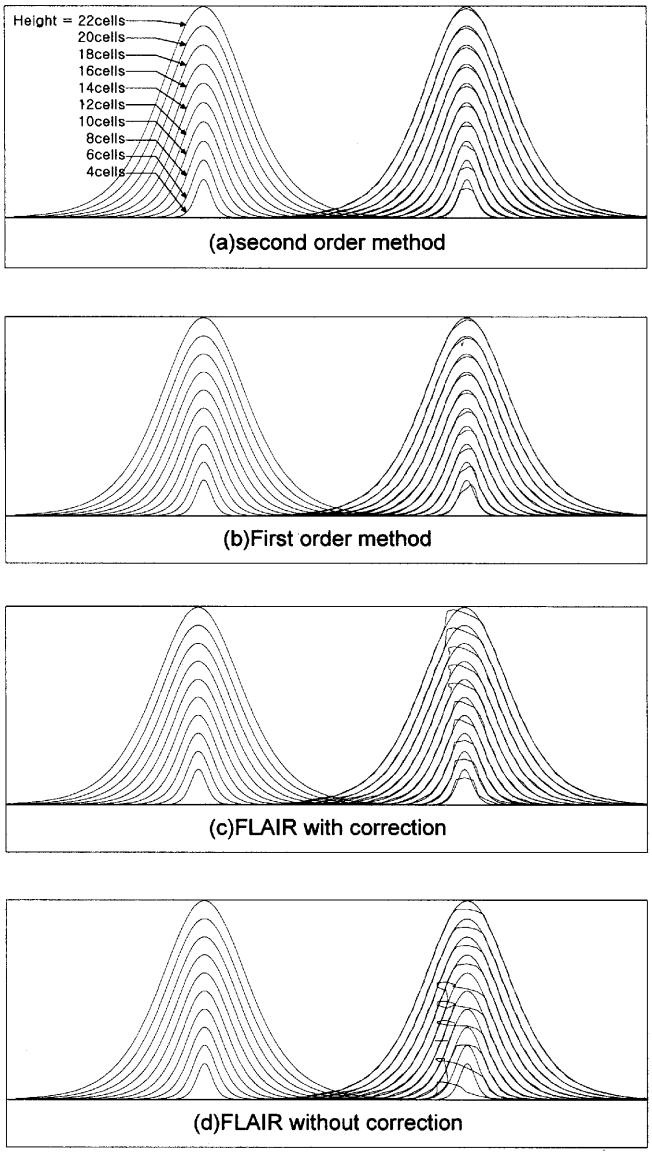

Figure 15. Reconstruction of solitary waves after 100 time steps of convection by each free surface convection model

To show the convection capability of each technique, various sizes of concentric circles are drawn with the analytic circles in Figure 14. This represents the volume fraction distribution after 100 time steps of convection.

The shapes of the free surface convected by the first-order approach show the most distortion. The shape of the FLAIR method almost coincides with the analytic circle at large diameter, but at small diameter the shape is seriously distorted by volume fraction diffusion. The shape of the second-order method is minimally distorted from the original for all circle diameters.

When not using correction techniques, the total volume change of each method remains within the order of $1{\cdot}0 \times 10^{-6}$ which corresponds to machine zero in the numerical analysis. However, the FLAIR method with correction logic shows various amounts of volume change ranging from the order of $1{\cdot}0 \times 10^{-3}$ for large diameters to the order of 1·0 for small diameters.

Therefore the total volume changes are not affected by the modelling of the free surface but are influenced instead by the convection method. Thus it is concluded that the total volume change cannot be used as an indication of the accuracy of a free surface model.

4.3. Convection capability of a solitary wave

To compare the performance of the convection methods for a geometry with a sharp corner, solitary wave convection is examined which is represented in the form of $y = h \sec h^2(kx) + y_0$. As a sample case the wave number k is assumed as $4{\cdot}0/h$ and the wave height h is varied from 4·0 to 16·0 times the length of one cell. The solitary wave is convected in the right-hand direction for 100 time steps with uniform velocity only in the x-direction as shown in Figure 15.

After 100 time steps of convection the FLAIR model shows the worst results among the three approaches for the maximum cell error and the root of square sum error (Figures 16 and 17). It may be reasoned that the boundary sloped line approach associated with the FLAIR method suffers from volume fraction diffusion at the initial time stage around the crest of the wave. The diffused volume fraction forces the FLAIR method to use the boundary sloped line approach for the convection of the rear face of the solitary wave, which accelerates the distortion of the volume fraction. Both the first- and second-order methods of this study show much better results than the FLAIR method. In

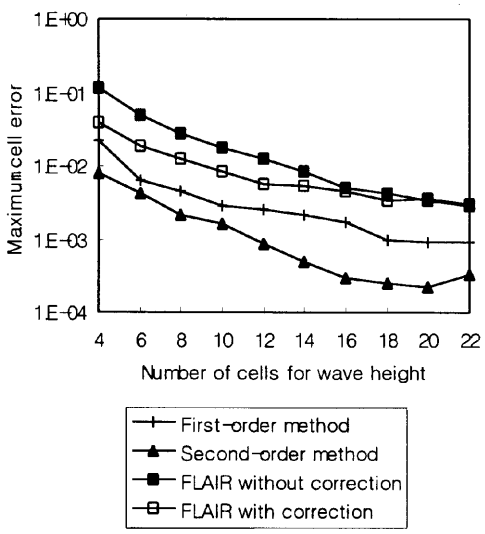

Figure 16. Maximum cell error versus solitary wave height after 100 time steps of convections

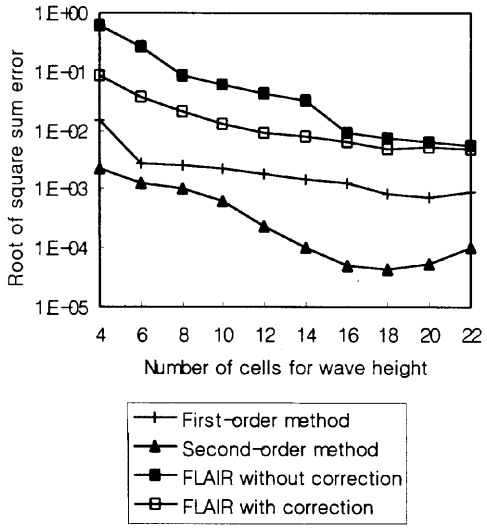

Figure 17. Root of square sum error versus solitary wave height after 100 time steps of convection

particular, the second-order model shows less error than the FLAIR method by an order of magnitude.

Based on a review of Figures 16 and 17, it is concluded that for a problem with large curvature of the free surface interface the second-order method can reduce the number of meshes by half relative to the first-order method. Compared with the FLAIR method, the second-order method reduces the mesh number by a factor of two to three. For all the methods evaluated, the volume changes remain almost within the machine-zero ranges.

However, whereas the semilogarithmic plots of errors in the circle problem versus mesh resolution indicate that the errors in the second-order method solution converge to zero at a more rapid rate than the errors in the first-order method, Figure 16 shows that the slopes of the error curves for both first- and second-order methods are nearly the same.

It is believed that the sharp edge still exists near the wave crest even if the number of cells in the solitary wave height increases within this calculational range.

Since the second-order curve is constructed by the combination of a defined volume fraction and two face slopes, the accuracy of the free surface reconstruction by the second-order method depends critically on the accuracy of the slopes. Therefore, if there is a rapid variation in volume fraction distribution, such as the crest of a wave existing within a cell, the first-order slope calculation method may be inappropriate. From the above results it is believed that the slopes of the error curves for both first- and second-order methods are nearly the same through the absolute errors have different values.

5. CONCLUSIONS

A new technique for the interface transport and reconstruction of a free surface has been developed for numerical models of the volume fraction method. The basic features of this technique are to represent the free surface and calculate the convective flux by utilization of a set of second-order linear curves. This technique was tested for various sizes of circles and solitary waves and a shaft keyhole advected with uniform velocity in the flow domain. For small curvature of the free surface, such as a circle with large diameter, the first-order approaches showed relatively close predictions to

those from the second-order method. For a large-curvature geometry, such as a circle with a relatively small diameter compared with the cell size or a solitary wave, the first-order approaches showed appreciable distortion of the shape and diffusion of the free surface. However, the second-order model consistently demonstrated accurate prediction capabilities of free surface convection even with a smaller number of cells.

It is also concluded that the total volume change cannot be used as an indicator of the accuracy of a free surface convection model, but the maximum cell convection error and the root of the square sum of every cell error should be used to measure the shape deformations.

In conclusion, it is recommended that for the reconstruction and convection of a free surface geometry with large curvature the second-order model should be used to reduce the computation time and to get better accuracy.

REFERENCES

1. J. F. Milthorpe and R. I. Tanner, 'Boundary element method for free surface viscous flows', *7th Australian Hydraulics and Fluid Mechanics Conf.*, Brisbane, August 1980.
2. M. Natori and H. Kawarada, 'Numerical solution of free surface drainage problem of two immiscible fluids by the boundary element method', *Jpn. J. Appl. Phys.*, **24**, 1359–1362 (1985).
3. H. C. Henderson, M. Kok and W. L. de Koning, 'Computer-aided spillway design using the boundary element method and non-linear programming', *Int. j. numer. meth. fluids*, **13**, 625–641 (1991).
4. R. Bonnerot and P. Jamet, 'Numerical computation of the free boundary for the problem by space–time elements', *J. Comput. Phys.*, **25**, 163–181 (1977).
5. D. R. Lynch, 'Unified approach to simulation on deforming elements with application to phase change problems' *J. Comput. Phys.*, **47**, 387–411 (1982).
6. P. Bach and O. Hassager, 'An algorithm for the use of the Lagrangian specification in Newtonian fluid mechanics and applications to free-surface flow', *J. Fluid Mech.*, **152**, 173–190 (1985).
7. I. S. Kang and L. G. Leal, 'Numerical solution of axisymmetric, unsteady free-boundary problems at finite Reynolds number. I. Finite-difference scheme and its application to the deformation of a bubble in a uniaxial straining flow', *Phys. Fluids*, **30** 1929–1940 (1987).
8. G. Ryskin and L. G. Leal, 'Numerical solution of free-boundary problems in fluid mechanics. Part 1. The finite-difference technique', *I. Fluid Mech.*, **148**, 1–17 (1984).
9. N. S. Asaithambi, 'Computation of free-surface flows', *J. Comput. Phys.*, **73**, 380–394 (1987).
10. F. H. Harlow and J. F. Welch, 'Numerical calculations of time-dependent viscous incompressible flow of fluid with free surface', *Phys. Fluids*, **8**, 2182–2189 (1965).
11. R. K.-C. Chan and R. L. Street, 'A computer study of finite-amplitude water waves', *J. Comput. Phys.*, **6**, 68–94 (1970).
12. H. Miyata, 'Finite difference simulation of breaking waves' *J. Comput. Phys.*, **65**, 179–214 (1986).
13. C. W. Hirt and B. D. Nichols, 'Volume of fluid (VOF) methods for the dynamics of free boundaries', *J. Comput. Phys.*, **39**, 201–225 (1981).
14. B. D. Nichols, C. W. Hirt and R. S. Hotchkiss, 'SOLA-VOF: a solution algorithm for transient fluid flow with multiple free boundaries', *Los Alamos Scientific Laboratory Rep. LA-8355*, 1980 (unpublished).
15. I. S. Partom, 'Application of the VOF method to the sloshing of a fluid in a partially filled cylindrical container', *Int. j. numer. meth. fluids*, **7**, 535–550 (1987).
16. W. F. Noh and P. Woodward, 'SLIC (simple line surface calculation)', in A. I. van de Vooren and P. J. Zandbergen (eds), *Lecture Notes in Physics*, Vol. 59, Springer, New York, 1976.
17. A. J. Chorin, 'Flame advection and propagation algorithm', *J. Comput. Phys.*, **35**, 1–11 (1980).
18. A. J. Chorin, 'Curvature and solidification', *J. Comput. Phys.*, **57**, 472–490 (1985).
19. D. L. Youngs, in K. W. Morton and M. J. Baineks (eds), *Numerical Methods for Fluid Dynamics*, Academic, New York, 1982.
20. N. Ashgriz and J. Y. Poo, 'FLAIR (flux line-segment model for advection and interface reconstruction)', *J. Comput. Phys.*, **93**, 449–468 (1991).
21. M. R. Spiegel, *Mathematical Handbook of Formulas and Tables in Schaum's Outline Series*, 1968.

